Title

Greenhouse gas emissions (CO2—CH4—N2O) along a large reservoir-downstream river continuum: The role of seasonal hypoxia

Journal

Limnology and Oceanography, 69(5)

ISSN

0024-3590

Authors

Wu, Zetao

Yu, Dan

Yu, Qibiao

et al.

Publication Date

2024-05-01

DOI

10.1002/lno.12544

Peer reviewed

LIMNOLOGY and OCEANOGRAPHY

ASLO

Limnol. Oceanogr. 9999, 2024, 1–15

doi: 10.1002/lno.12544

Greenhouse gas emissions (CO_2–CH_4–N_2O) along a large reservoir-downstream river continuum: The role of seasonal hypoxia

Zetao Wu,[1,2] Dan Yu,[1,2] Qibiao Yu,[1,2] Qian Liu,[3] Mingzhen Zhang,[1,2] Randy A. Dahlgren,[4] Jack J. Middelburg,[5] Liyin Qu,[6,7] Quanlong Li,[1,2] Weidong Guo,[1,6*] Nengwang Chen[1,2*]

[1]State Key Laboratory of Marine Environment Science, Xiamen University, Xiamen, China
[2]Fujian Provincial Key Laboratory for Coastal Ecology and Environmental Studies, College of the Environment and Ecology, Xiamen University, Xiamen, China
[3]Frontiers Science Center for Deep Ocean Multispheres and Earth System, and Key Laboratory of Marine Chemistry Theory and Technology, Ministry of Education, Ocean University of China, Qingdao, China
[4]Department of Land, Air and Water Resources, University of California, Davis, California, USA
[5]Department of Earth Sciences, Utrecht University, Utrecht, The Netherlands
[6]College of Ocean and Earth Sciences, Xiamen University, Xiamen, China
[7]National and Local Joint Engineering Research Center of Ecological Treatment Technology for Urban Water Pollution, Wenzhou University, Wenzhou, China

Abstract

Recent studies suggest that hypolimnetic respiration may be responsible for greenhouse gas (GHG) emissions from deep reservoirs. Currently, quantitative evaluation of aerobic vs. anaerobic processes and priming (enhanced processing of organic matter due to the addition of labile carbon) in regulating GHG production and emissions across the reservoir-downstream continuum remains largely unknown. High-resolution, annual time-series observations in a large, subtropical reservoir (Shuikou) experiencing seasonal hypoxia in southeast China indicate that aerobic hypolimnetic CO_2 production dominated in most periods of the stratified spring/summer with higher rates at higher temperatures. In addition, anaerobic production of hypolimnetic CO_2 occurred in the late stratified spring/summer period, which stimulated hypolimnetic production of CH_4 and N_2O. Incubation experiments showed that priming in spring enhanced both aerobic and anaerobic production of excess GHGs. A late spring flood event generated the highest daily efflux of CO_2 through the flushing of GHG-enriched hypolimnion waters. Turbine degassing contributed 59%, 93%, and 63% of annual CO_2, CH_4, and N_2O effluxes, respectively. Moreover, annual downstream GHG emissions were similar to those in the transition/lacustrine zone of the Shuikou reservoir. Diurnal variation observations revealed net CO_2 emissions even during algal bloom seasons. The reservoir-downstream river continuum was a year-round source of GHGs (218.5 ± 18.9 Gg CO_2-equivalent yr^{-1}; CO_2 contributed 91%). However, the loss of oxygen also leads to increased production and storage of recalcitrant dissolved organic carbon (RDOC). Thus, identifying mechanisms controlling both GHG emissions and RDOC production is crucial to constrain the carbon neutrality issue of hydroelectric reservoirs in the context of climate change mitigation strategies.

Globally, more than 70,000 large dams (> 15 m height) with ~ 500,000 km^2 of reservoir surface area have been built to meet the growing demand for renewable energy and irrigation/drinking water sources (Wang et al. 2022). These anthropogenic impoundments greatly enhance the heterotrophic metabolism of degradable organic matter in reservoirs

*Correspondence: wdguo@xmu.edu.cn; nwchen@xmu.edu.cn

Additional Supporting Information may be found in the online version of this article.

Zetao Wu and Dan Yu are the co-first authors of the article.
Author Contribution Statement: Z.W.: Investigation—sampling and experiments (lead); writing—original draft (equal); formal analysis—statistics (equal); visualization—figure creation (equal). D.Y.: Writing—original draft (equal); formal analysis—statistics (equal); visualization—figure creation (equal); writing—review and editing (equal). Q.Y.: Investigation—sampling (supporting). Q.L.: Writing—original draft (supporting); writing—review and editing (supporting). M.Z.: Investigation—sampling (supporting). R.A.D.: Writing—review and editing (equal). J.J.M.: Writing—review and editing (equal). L.Q.: Writing—original draft (supporting); writing—review and editing (supporting). Q.L.: Methodology (supporting). W.G.: Conceptualization (equal); writing—original draft (equal); writing—review and editing (equal). N.C.: Conceptualization (equal); supervision (lead); writing—original draft (supporting); writing—review and editing (equal).

owing to their longer water residence times (WRTs) (Maavara et al. 2017; Qu et al. 2022). A potentially adverse effect is the production and emissions of greenhouse gases (GHGs; i.e., CO_2, CH_4, and N_2O) (Barros et al. 2011), offsetting the positive green benefits of hydropower (Kumar et al. 2019; Paranaíba et al. 2021). However, current estimates of global GHG emissions from hydroelectric reservoirs are primarily restricted to reservoir water surfaces (Barros et al. 2011; Deemer et al. 2016). Recent studies demonstrated large amounts of unaccounted emissions of GHGs by hypolimnetic water release and turbine degassing (Fearnside 2002; Soued and Prairie 2020; Calamita et al. 2021), accompanied by the export of "excess" nutrients and recalcitrant dissolved organic carbon (RDOC) to downstream rivers (Carey et al. 2022; Qu et al. 2022). Hence, there could be a substantial underestimation of GHG emissions if hypolimnetic mineralization processes and their influence on the entire reservoir-river continuum are not completely assessed (Soued et al. 2022).

During thermal stratification periods of reservoirs, there is active hypolimnetic oxygen consumption involving aerobic and anaerobic stages (Carey et al. 2018; Han et al. 2018; Wentzky et al. 2019). During the aerobic stage, oxygen is aerobically consumed by microbial degradation of bioavailable organic matter, which is generally considered the dominant process for CO_2 production in aquatic systems (Richey et al. 1988; Atkins et al. 2013). Continued hypolimnetic oxygen consumption following stratification could eventually lead to the occurrence of hypoxia and even anoxia (dissolved oxygen [DO] < 0.2 mg L^{-1}) in bottom waters and sediments of reservoirs (Yan et al. 2021), which may initiate the anaerobic degradation of organic matter and in this way sustain production of CO_2 (Cai et al. 2003; Krumins et al. 2013) and other GHG gases (e.g., CH_4, N_2O) (Rinta et al. 2015). In contrast to tropical reservoirs with persistent thermal stratification and long-lasting hypoxia (Abril et al. 2005; Soued and Prairie 2020), subtropical and temperate reservoirs commonly experience seasonal stratification (hypoxic)–overturn (oxic) cycles. However, how seasonal hypolimnetic hypoxia regulates the production of GHGs in subtropical reservoirs remains largely unknown. Moreover, whether and how hypolimnetic temperature regulates reservoir GHG production/emissions needs further investigation.

The addition of labile organic matter could induce priming, that is, degradation of otherwise refractory organic matter (Guenet et al. 2010; Bianchi 2011). This priming effect has been found to increase mineralization resulting from inputs of both allochthonous and autochthonous organic matter (e.g., in lakes of the Qinghai–Tibet Plateau) (Yang et al. 2023). Thus, input of labile organic matter from watershed runoff or decomposition of algal blooms could enhance production and emissions of GHGs in reservoirs, which has not attracted enough attention.

Storm-induced flood events exhibit contrasting hydrological processes from baseflow in regulating CO_2 and CH_4 emissions of reservoirs (Li et al. 2022). The interruption of stratification results in resupply of oxygen to the hypolimnion layer and a pulse input of terrigenous organic matter (Yan et al. 2021; Zhou et al. 2021*b*), which could fuel hypolimnetic mineralization and, therefore, GHG production due to substrate supply and potential priming effect. In addition, flood events increase the surface water velocity and water–air GHG exchange. The sharp increase in stormflow may further enhance the flushing of GHGs from reservoirs, resulting in strong turbine degassing and downstream emissions. Due to logistical difficulties in obtaining high-quality field measurements, little is known about storm event effects on GHG emissions along the reservoir-river continuum.

The water–air exchange flux of GHGs largely depends on GHG concentrations in the reservoir epilimnion (i.e., the surface layer) because atmospheric concentration is rather invariant (Guérin et al. 2007; Zagarese et al. 2021). The gradient in GHG concentrations between air and water may show strong diurnal variability in magnitude or sign, as daytime is usually dominated by photosynthesis, while respiration dominates during nighttime. For example, the CO_2 efflux in Ross Barnett Reservoir (Mississippi, USA) at night is about 70% higher than that during daytime (Liu et al. 2016). This makes diurnal time-series observations of GHG exchange fluxes in reservoirs an essential prerequisite, as using only daytime observation data may result in a systematic underestimation of 9–25% (Ran et al. 2022). Thus, diurnal variations cannot be ignored when spatial variation of water–air GHG flux exchanges in river reservoirs are estimated across large time spans, such as an annual cycle (Paranaíba et al. 2021).

China is one of the largest hydropower producers in the world (Tarroja et al. 2014; Lu et al. 2020). Shuikou (SK) reservoir, the largest dam/reservoir in southeast China located on the Min River, is a typical reservoir owing to its consistent occurrence of seasonal hypolimnetic hypoxia and storm-induced flood events under an Asian monsoon climate (Yan et al. 2021; Qu et al. 2022). Herein, we conducted comprehensive investigations of GHGs across the SK reservoir-downstream Min River continuum in different seasons using multiple strategies: high-resolution observations covering the transition and lacustrine zones of the reservoir, time-series diurnal monitoring of surface water and vertical profile observations at the lacustrine site, and lab incubation experiments to assess priming and mineralization rates. The objectives of this study were to: (1) explore the spatial–temporal patterns of GHG production and emissions under a seasonal stratification-overturn cycle; (2) examine the role of aerobic and anaerobic respiration in hypolimnetic CO_2, CH_4, and N_2O production and the relationship of CO_2 production with temperature; (3) test whether priming effects enhance hypolimnetic CO_2 production; and (4) quantify the spatio-temporal hot spots for GHG emissions across the entire reservoir-river continuum. This study highlights the urgent need to address hypolimnetic processes in reservoirs and lakes

to improve the accounting of GHG budgets across the land–ocean interface at regional and global scales.

Materials and methods

Description of the study area

The Min River is the third largest river in terms of runoff to the China Seas (Supporting Information Fig. S1a), with a mean annual discharge of 3.9×10^{10} m^3. The watershed has a subtropical humid monsoon climate with a mean annual air temperature of 16–20°C and elevated precipitation in the distinct wet season from April to September. The mean annual precipitation is 1700 mm, with flood events mainly occurring in late spring (May–June) (Supporting Information Fig. S1b). The daily average wind speed obtained from 20 national meteorological stations in the watershed ranged between 0.2 and 6.2 m s^{-1} in 2020–2021 and displayed small spatial and seasonal variations.

SK reservoir (116°23′–119°35′E, 25°23′–28°16′N) was built in the 1990s on the Min River with a storage capacity of 2.6 billion m^3 and a full-reservoir water surface area of 97 km^2. The average depth of the transition zone was ~ 30 m, whereas the deeper lacustrine zone was ~ 55 m; the hypolimnetic release point was ~ 30 m below the water surface. Average WRTs were 12.9 ± 8.3 d (mean ± std dev) for summer (July 2020), 45.6 ± 14.3 d for fall (November 2020), 43.0 ± 0.7 d for winter (January 2021), 33.1 ± 12.4 d for spring (April 2021), and 6.6 ± 3.1 d for the spring flood-falling period (June 2021). Definitions for the specific seasons/periods are described in Supporting Information Text S1. SK reservoir is a mildly eutrophic system, and long-term seasonal hypoxia expands from the bottom to near-surface waters (Yan et al. 2021).

In situ monitoring and sampling

To evaluate the stratification status and oxygen evolution of SK reservoir, time-series of in situ monitoring of water temperature, DO and chlorophyll *a* (Chl *a*) at a 1-h interval in surface (0.5 m) and hypolimnetic layers of the transition (site Z3, 15 m depth) and lacustrine (site S4, 45 m depth) zones were conducted using buoys equipped with a multiparameter water quality sonde (YSI EXO2) along with regular data calibration/quality assurance (Supporting Information Text S2) from 1 July 2020 to 30 June 2021. An index of relative thermal resistance to mixing (RTRM) was calculated, which indicates stratification (> 50) or mixing (< 50) of the reservoir (Supporting Information Text S3).

To estimate spatial variations of excess dissolved carbon dioxide (ΔCO_2; i.e., carbon dioxide above equilibrium with air) and water–air CO_2 flux exchanges, longitudinal boat surveys using underway-pumping measurement of surface pCO_2 and temperature covering the entire transition and lacustrine zones of SK reservoir (back and forth from Z3 to S1) were conducted once per season/period in summer (July 2020), fall (November 2020), winter (January 2021), spring (April 2021) and a spring flood-falling period (June 2021) (Supporting Information Fig. S1b). To examine diurnal variations, a 24-h observation of surface pCO_2 and temperature was performed at S4 (center of lacustrine zone) following the boat underway-pumping surveys (Supporting Information Text S4).

Water column vertical profiles of temperature, DO, Chl *a*, pH (± 0.01), specific conductivity, and turbidity were measured at three sites in the transition (Z1, Z2, and Z3) and lacustrine (S1, S4, and S7) zones of SK reservoir by YSI EXO$_2$ once per season/period, with data calibration/quality assurance (Supporting Information Text S2). The oxygen departure from atmosphere equilibrium ($O_{2\_observed} - O_{2\_equilibrium}$, μmol L^{-1}) was defined as ΔO_2 (Vachon et al. 2020).

Water samples from 7 to 10 m depths were collected by Niskin bottles at three sites (S1, S4, and S7) in the lacustrine zone of SK reservoir in four seasons and the spring flood-falling period. Surface water samples were also collected at one site in the transition zone (Z3) and five sites (D1–D5) in the downstream Min River on each cruise. Diurnal time-series water samples were collected at 1–3 h intervals for dissolved inorganic carbon (DIC), CH_4, and N_2O analysis at S4. For nutrients, a subsample was filtered through a GF/F membrane (0.7 μm). Dissolved and particulate organic carbon data from the study period are available from Qu et al. (2022). Sample replication and preservation protocols are described in Supporting Information Text S5.

Incubation experiment

Samples were incubated to quantify CO_2 and CH_4 production, DO consumption and to determine if there was production of excess CO_2 due to a priming effect from mixing surface DOM with hypolimnetic DOM during the overturn period (Bianchi 2011). Incubation experiments were conducted with surface, bottom, and mixed (30% surface + 70% bottom) water samples collected at S4 during fall (November 2020) and winter (January 2021). A priming effect is identified if the CO_2 production rate (μmol L^{-1} d^{-1}) of the mixed group was higher than the weighted-average CO_2 production rate of surface (30%) and bottom (70%) waters, with the difference defined as δCO_2. For comparison, a similar incubation experiment was conducted during the stratified spring period (April 2021) as more bio-labile surface particulate and dissolved organic matter were available (Qu et al. 2022). The biodegradable substrates in the spring samples completely consumed the O_2 in the incubation system, thus providing an opportunity to simulate the shift from aerobic to anaerobic respiration. The CH_4 concentrations were measured along with CO_2 to quantify net methane production. Experimental details and calculation of the priming effect are described in Supporting Information Text S6. The standard error for the priming effect was calculated to examine the uncertainty caused by both variation among subsamples and production rate at different timesteps.

Laboratory analysis

DIC concentration was determined using a LI 7000 infrared analyzer (Applo AS-C2), with a precision of $\pm 2\ \mu mol\ kg^{-1}$. Concentrations of dissolved CH_4, N_2O, and CO_2 in incubations were measured by gas chromatography (Agilent 7890A), with a relative error < 1.5%. Ammonium (NH_4–N), nitrite (NO_2–N), nitrate (NO_3–N), and dissolved reactive phosphorus concentrations were measured by continuous flow colorimetry (SEAL AutoAnalyzer 3) with relative errors < 5%.

Water–air GHG flux calculations

To calculate gas fluxes, excess CO_2 (ΔCO_2, $\mu mol\ L^{-1}$) was first defined as the departure of dissolved CO_2 from atmospheric equilibrium and calculated following Zhai et al. (2005). Similarly, ΔCH_4 ($\mu mol\ L^{-1}$) and ΔN_2O ($\mu mol\ L^{-1}$) were defined as the departure of free dissolved CH_4 and N_2O from atmospheric equilibrium and calculated as the concentration differences between dissolved CH_4 (N_2O) and atmospheric equilibrated CH_4 (N_2O). Water–air GHG flux (F; $mmol\ m^{-2}\ h^{-1}$) was then estimated as $k_x \times \Delta CO_2$ (ΔCH_4, ΔN_2O) $\times\ 10^{-2}$, where k_x ($cm\ h^{-1}$) is the gas transfer value for CO_2, CH_4, and N_2O at the observed temperature and the factor 10^{-2} provides unit consistency (Supporting Information Text S7).

GHG efflux budgets for reservoir-downstream continuum

There are three distinct segments for GHG degassing from the reservoir-downstream continuum (i.e., reservoir, turbine, and downstream river). Daily degassing CO_2 (CH_4 and N_2O) efflux (E; $t\ d^{-1}$) in the reservoir and downstream segments during each season/period was quantified as $E = F \times S \times M_x \times 0.042 \times 10^{-3}$, where F is the average water–air CO_2 (CH_4, N_2O) flux ($mmol\ m^{-2}\ h^{-1}$) of each segment; S (km^2) is the water surface area (20, 17, and 25 km^2, for transition, lacustrine and downstream river, respectively), M_x ($g\ mol^{-1}$) is the mole mass of CO_2 (CH_4 and N_2O); the factor 0.042×10^{-3} is to convert to the unit of $t\ d^{-1}$. The emissions for each season/period (Gg) were calculated as daily efflux ($t\ d^{-1}$) times its duration (d) (Supporting Information Text S1) of that season, together with a factor of 10^{-3} for unit consistency. The annual efflux ($Gg\ yr^{-1}$) was determined as the sum of all seasonal emissions (Gg) for the year.

CO_2 and CH_4 degassing effluxes by turbines were estimated based on the concentration difference between hypolimnion and downstream waters, while the degassing efflux of N_2O was estimated using the percentage degassing efflux of CH_4 to total reservoir CH_4 release efflux (Supporting Information Text S8), as downstream N_2O dynamics appeared to be affected by input from domestic wastewater discharge of local villages (Yan et al. 2023). CH_4 and N_2O effluxes were converted to 27 and 273 times the global warming potential (GWP) of CO_2 (CO_2-equivalent, CO_2-eq) over a 100-yr time horizon (IPCC 2021).

Other data processing and statistical analyses

In situ production rates for CO_2 ($\mu mol\ L^{-1}\ d^{-1}$) in the hypolimnion of SK reservoir were quantified from the oxygen utilization rate (OUR): $PR = \Delta CO_2/(O_{2\_equlibrium}\text{-}O_{2\_observed}) \times OUR$, where ΔCO_2 ($\mu mol\ L^{-1}$) is the excess CO_2; $O_{2\_equlibrium}$ and $O_{2\_observed}$ ($\mu mol\ L^{-1}$) are the equilibrium and observed O_2 concentration, respectively; OUR ($\mu mol\ L^{-1}\ d^{-1}$) is the average oxygen consumption magnitude of the hypolimnion during the WRT. This approach was similar to the method used to determine in situ production rates for the humic-like fluorescent DOM–$FDOM_H$ (Qu et al. 2022). This estimation can only be applied to stratification periods having no oxygen supplements. Maps were drawn using ArcGIS 10.8, and data were plotted using Origin and EXCEL. All statistical tests were performed with SPSS 26.0. Pearson correlation and ANOVA were used to evaluate relationships and differences at a p level of 0.05.

Results

Physicochemical parameters in the reservoir

Water temperature, DO, and Chl *a* showed seasonal and spatial variation in the transition and lacustrine zones of SK reservoir (Fig. 1; Supporting Information Fig. S3). The temperature difference between the surface and bottom layers was much larger in the deeper lacustrine zone than in the shallower transition zone in all periods, except for the falling phase of the late-spring flood event when the whole reservoir was well-mixed (i.e., RTRM ≤ 50) (Fig. 1a,b). Conversely, the transition zone was in a mixed status throughout most of the year, except for mid-July and early October (Fig. 1b). In the lacustrine zone, the larger temperature difference in spring and summer (8°C and 6°C) corresponded to a persistent stratified status (i.e., RTRM > 50) (Fig. 1b; Supporting Information Fig. S3a,d). The hyperpycnal flow and/or overturning process in early autumn, indicated by the higher specific conductivities in the bottom layer (Supporting Information Fig. S4), changed the stratification status to well-mixed in winter.

The DO concentration in SK reservoir decreased with depth in all seasons except for the flood period (Supporting Information Fig. S3). In the surface layer, DO was high in spring (6.43–11.51 $mg\ L^{-1}$) and summer (7.52–9.32 $mg\ L^{-1}$) and was oversaturated in certain areas of the lacustrine zone. In contrast, surface DO was below saturation in fall (2.46–6.89 $mg\ L^{-1}$, DO%: 41.5–60.6) and winter (4.53–7.68 $mg\ L^{-1}$, DO%: 53.4–64.7). In the lacustrine zone, hypolimnetic hypoxia (DO < 2 $mg\ L^{-1}$) started in August with a short disappearance in October, but also re-occurred during April. The bottom layer reached anoxia status in late summer (August and September) and late spring (mid-April to mid-May) (Fig. 1d). There was only occasional hypoxia in late summer within the shallower transition zone, while the hypolimnetic oxygen was well above hypoxia during the fall, winter and flood periods (Supporting Information Fig. S3b–e).

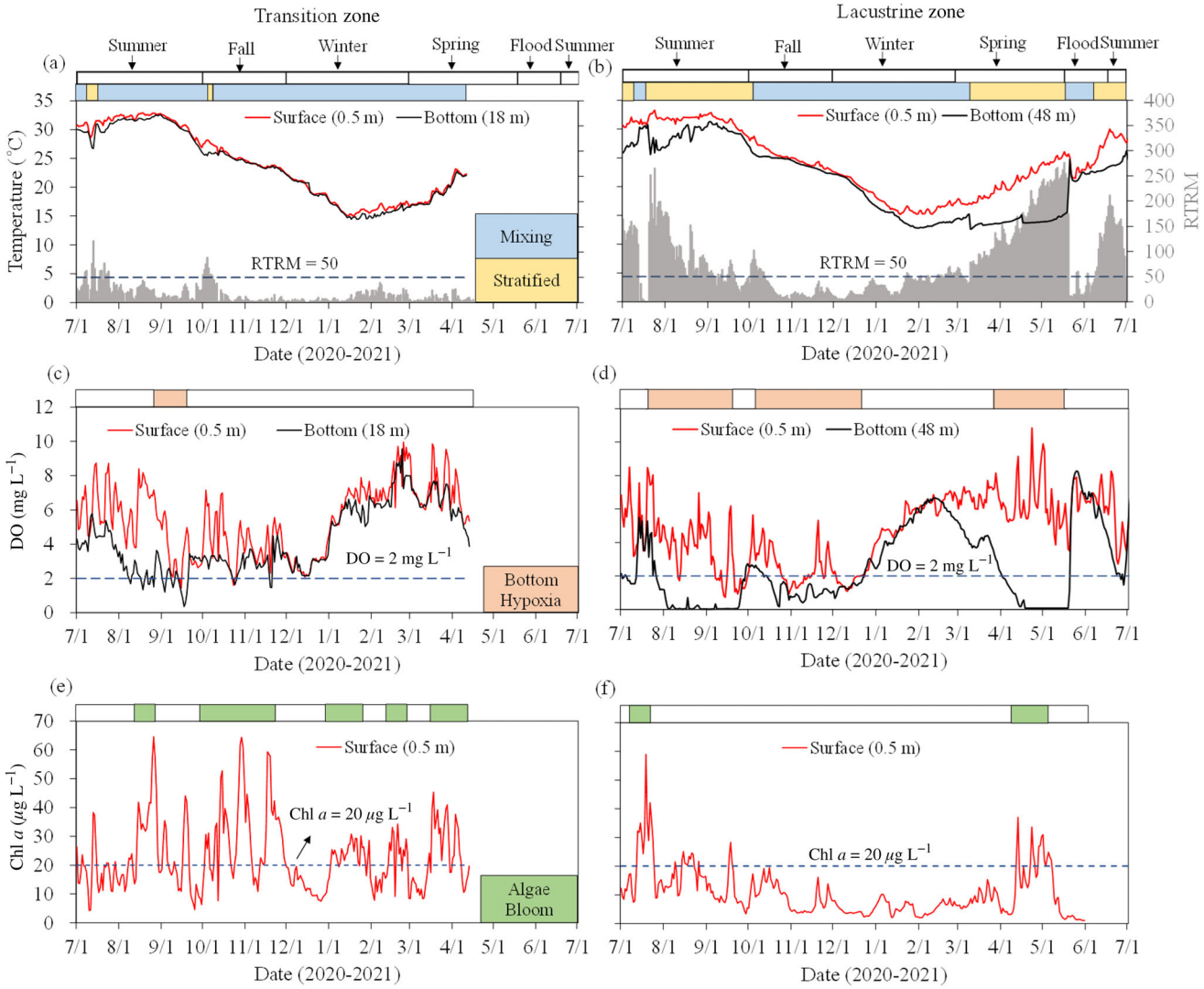

Fig. 1. Time-series data for surface and bottom temperature (**a**, **b**), DO (**c**, **d**), and surface Chl *a* (**e**, **f**) in transition and lacustrine zones (Z3 and S4) of SK reservoir. A stratification index RTRM (relative thermal resistance to mixing, gray shaded) of 50 was used to divide stratified vs. mixed periods in the reservoir. Bottom DO < 2 mg L^{-1} was defined as hypoxia and Chl *a* > 20 μg L^{-1} represents the algae bloom events.

Surface algal blooms (Chl *a* > 20 μg L^{-1}) occurred within all seasons in the transition zone vs. only in spring and summer in the lacustrine zone (Fig. 1e,f). The Chl *a* decreased in fall and reached its lowest levels in winter (Fig. 1f). During the flood-falling period, surface Chl *a* at S4 was recorded at > 20 μg L^{-1} (Supporting Information Fig. S5a). Chl *a* showed very low concentrations below the euphotic zone in spring and summer (Supporting Information Fig. S3a,d). However, Chl *a* in fall and winter showed relatively high values (1.2–7.0 μg L^{-1}) in the deeper layer of the transition zone due to water mixing (Supporting Information Fig. S3b,c). In particular, the hyperpycnal flow from upstream, characterized by lower temperature and higher DO and Chl *a*, was evident from the transition to lacustrine zones along the bottom layer in fall and winter.

Distribution of pH, DIC, and ΔGHGs in the reservoir

Vertical profiles of pH, DIC, and ΔGHGs (excess concentrations relative to atmosphere) in SK reservoir are shown in Fig. 2. DIC and ΔCO_2 in surface water of the lacustrine zone were higher than those in the transition zone in all investigated periods, but the ΔCH_4 and ΔN_2O concentrations showed similar levels among the two zones. The vertical distributions of pH, DIC, and ΔGHGs were variable during the different temporal periods in the lacustrine zone. In spring and late summer, the concentration of CO_2 in the surface water was below atmospheric equilibrium level (negative ΔCO_2), while DIC and ΔCO_2 concentrations reached their highest level at depths deeper than 30 m due to stratification (Fig. 1b). The ΔCH_4 and ΔN_2O concentrations in the bottom layer during spring/summer were much higher than other periods due

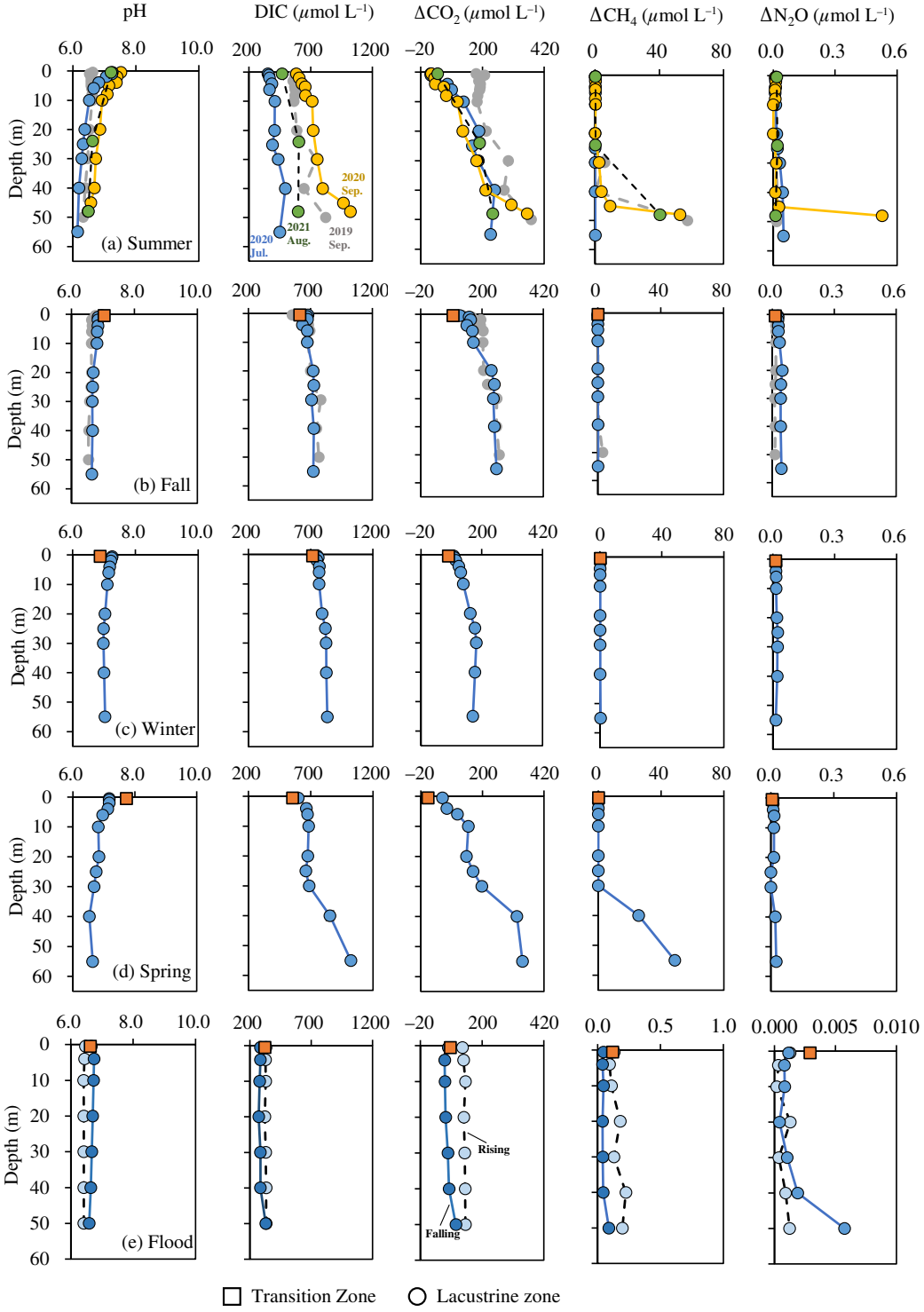

Fig. 2. Vertical distributions of pH, DIC, ΔCO_2, ΔCH_4, and ΔN_2O in SK reservoir during the four seasons (**a–d**) and flood period (**e**). Squares represent data from the transition zone, and circles represent data from the lacustrine zone. Blue circles in (**a**) indicate data from July 2020; yellow circles in (**a**) from September 2020; gray circles in (**a**) and (**b**) from September and October 2019; green circles in (**a**) from August 2021; light blue circles in (**e**) are flood-rising period and dark blue circles in (**e**) are the flood-falling period.

to the anaerobic conditions at this time. Concentrations of DIC, ΔCO_2, and ΔCH_4 in the hypolimnion increased as summer progressed, with the highest concentrations in late summer (Fig. 2a). During the fall, winter, and flood periods, the vertical concentrations of parameters were more evenly distributed. The autumn ΔCO_2 in the bottom layer was lower

than the summer, whereas the average ΔCO_2 concentration throughout the water column was slightly higher. The ΔGHGs reached their lowest levels during the flood event falling period. A much lower pH was observed in the deeper layer (> 5 m) of the reservoir at this time and in early summer.

CO_2 production during aerobic and anaerobic conditions: Incubation experiments

During all incubation experiments, CO_2 production occurred, with higher production rates in the bottom than in surface waters in the winter season ($p < 0.05$) (Fig. 3). In fall and winter, O_2 concentrations estimated from CO_2 production declined but remained above 10 μmol L^{-1} during the 15-d incubation (Fig. 3a,d). Estimated O_2 levels were above zero even when using the upper limit of reported O_2/CO_2 ratios (1.61). Accordingly, aerobic CO_2 production rates were 1.19 ± 0.37–2.08 ± 0.34 μmol L^{-1} d^{-1} in fall and 2.01 ± 0.15–2.95 ± 0.17 μmol L^{-1} d^{-1} in winter (Supporting Information Table S1). In contrast, O_2 concentrations were estimated to become zero after 5–10 d in incubations with bottom and mixed group waters in spring (Fig. 3h), resulting in a shift from hypoxic to anaerobic conditions. Overall CO_2 production rates in spring (3.61 ± 0.71–9.18 ± 0.70 μmol L^{-1} d^{-1}) were higher than those in fall and winter seasons ($p < 0.05$), with especially higher production rates of 8.24 μmol L^{-1} d^{-1} for bottom water and 10.86 μmol L^{-1} d^{-1} for mixed waters during the late anaerobic stage (Supporting Information Table S1). The indicator for a potential priming effect, δCO_2, was significant in stratified spring (3.63 ± 0.52–4.58 ± 0.61 μmol L^{-1} d^{-1} among different timesteps), with an overall value of 4.09 ± 1.27 μmol L^{-1} d^{-1} for the whole experiment. On the contrary, the overall δCO_2 in fall (0.05 ± 0.52 μmol L^{-1} d^{-1}) and winter (0.64 ± 0.42 μmol L^{-1} d^{-1}) was small. CH_4 concentrations were less than 0.04 μmol L^{-1} and generally decreased during incubation in the aerobic fall and winter samples and in surface water during spring (Fig. 3c,f). CH_4 decreased from higher levels (0.50 ± 0.13–1.27 ± 0.36 μmol L^{-1}) to zero before O_2 was consumed in the spring bottom and mixed waters. However, CH_4 was quickly produced at the onset of anaerobic conditions, especially for bottom waters (Fig. 3i).

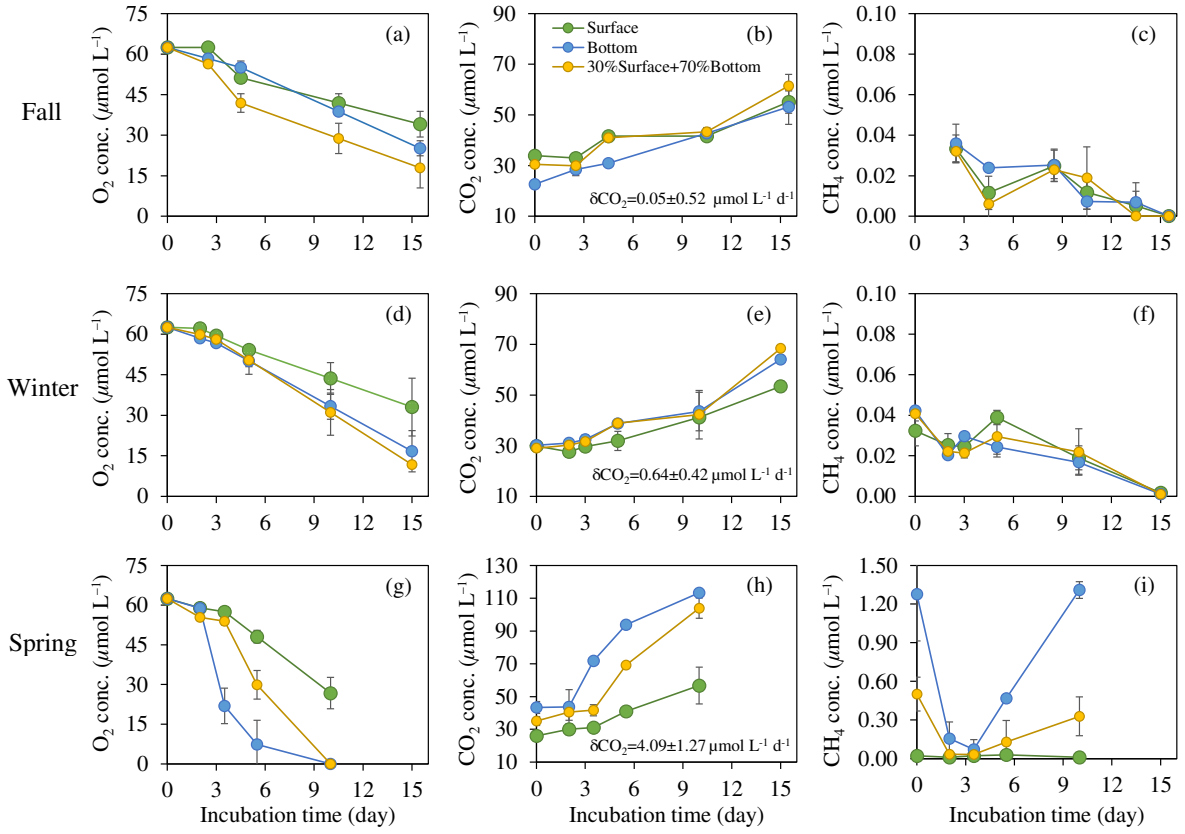

Fig. 3. Variation (mean ± std; $n = 3$) of estimated O_2 (**a**, **d**, **g**), measured CO_2 (**b**, **e**, **h**) and CH_4 (**c**, **f**, **i**) concentrations during incubation experiments. O_2 concentrations and their error bars are calculated using an O_2/CO_2 ratio of 1.20 (range = 1.11–1.61 for freshwater systems; Wang et al. 2014). The dashed line separates the preincubation from the remaining incubation that was included in the estimation of the priming effect. As an indicator for the priming effect, δCO_2 was calculated as the difference between the CO_2 production rate of the mixed water group and the weighted-average CO_2 production rate of the surface (30%) and bottom (70%) water groups.

Variation of surface GHG concentrations and fluxes

The 24-h time-series observations at S4 revealed larger diurnal variations of surface pCO_2 concentrations and water–air CO_2 fluxes during the stratified spring (83–3897 μatm, −0.5 to 4.7 mmol m^{-2} h^{-1}), summer (404–4210 μatm, 0.4–4.6 mmol m^{-2} h^{-1}) and spring flood-falling period (55–2501 μatm, −0.5 to 3.1 mmol m^{-2} h^{-1}), compared to the well-mixed fall (3750–5565 μatm, 3.3–6.3 mmol m^{-2} h^{-1}) and winter (3780–4116 μatm, 3.9–4.5 mmol m^{-2} h^{-1}) time periods (Fig. 4; Supporting Information Fig. S5b). Surface ΔCO_2 showed a similar pattern as pCO_2 among seasons. The pCO_2 and CO_2 fluxes at certain daytime periods were low due to photosynthesis, whereas continuous respiration, especially during nighttime and early morning, resulted in elevated pCO_2 and CO_2 fluxes. This resulted in 1.55 (spring), 1.69 (summer), and 2.40 (flood-falling period) times higher average pCO_2 values across the whole 24-h period compared to the daytime period during stratified periods. The CO_2 fluxes were only 1.05–1.06 times higher in fall and winter seasons due to smaller diurnal pCO_2 variations (Supporting Information Fig. S5b). Contrary to ΔCO_2, surface ΔCH_4 and ΔN_2O levels showed only slight differences between daytime and nighttime during the four seasons (Supporting Information Fig. S6). To alleviate the significant underestimation of water–air GHG fluxes resulting from the use of only daytime data (Calamita et al. 2021), the daily GHG fluxes from SK reservoir and the downstream river are all reported on a 24-h basis (Supporting Information Text S9).

The SK reservoir and its downstream river were a GHG source to the atmosphere on both seasonal and annual timescales (Table 1), with an annual GHG efflux of 218.5 ± 18.9 Gg CO_2-eq yr^{-1}, of which CO_2, CH_4, and N_2O accounted for 91%, 5%, and 4%, respectively. During the spring flood-rising period, the reservoir-downstream continuum had the highest daily CO_2 efflux (~ 3657 t CO_2-eq d^{-1}), which was 9, 5–8, and 9–12 times those of the flood-falling, stratified and mixed periods, respectively (Supporting Information Table S2). Throughout the annual cycle, CO_2 effluxes from the continuum had the highest value during the stratified summer (40%), and the spring flood period contributed 14% but accounted for only 8% of the duration. In particular, turbine degassing contributed the greatest CO_2 efflux in all periods (spring flood period: 68–73%; stratified: 55–69%; mixed: 33–50%; annual: 59%). The CO_2 efflux in the downstream river was comparable to that in the lacustrine and transition zones in spring and winter, but was 1.6–2.4 times greater in the summer and fall. A total of 10.7 Gg CO_2-eq yr^{-1} CH_4 was released from the continuum throughout the year, 93% of which degassed from the turbine. Moreover, 78% and 16% of annual CH_4 efflux occurred in spring and summer, of which 84–97% was degassed from the turbine (Table 1).

The daily CH_4 efflux from the continuum was high in spring (107.2 t CO_2-eq d^{-1}) and the spring flood-rising period (36.7 t CO_2-eq d^{-1}). The spring/summer values were 10–23 times those in the fall, winter, and flood-falling period (Supporting Information Table S2). N_2O effluxes from the continuum were the highest in summer and fall. A total of 38–78% (annual mean of 63%) of N_2O degassing occurred from the turbine as estimated via the methane degassing percentages, whereas the downstream segment contributed 6–25%, partly derived from contributions of local anthropogenic

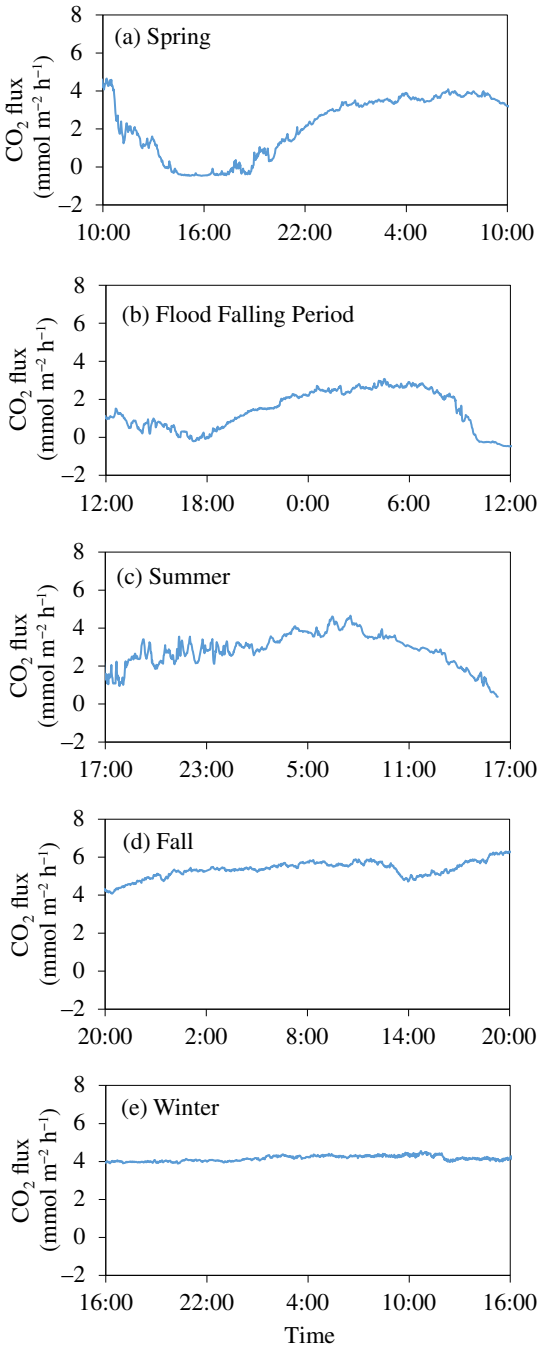

Fig. 4. Diurnal variation of water–air CO_2 fluxes during different periods at site S4 in SK reservoir.

Table 1. Annual CO_2-equivalent emissions (Gg CO_2-eq) within the SK reservoir-downstream river continuum from 1 July 2020 to 30 June 2021.

GHGs	Item	Spring	Summer	Fall	Winter	Flood rising	Flood falling	Annual
CO_2	Transition zone	5.63	7.12	2.53	5.59	2.39*	0.78	24.03
	Lacustrine zone	5.22	6.38	3.88	6.27	2.03	0.97	24.75
	Turbine	20.79	55.63	12.30	9.18	13.35	6.95	118.20
	Downstream	5.83	11.70	6.08	7.18	0.52	1.48	32.80
	Total	37.47	80.82	24.79	28.22	18.28	10.19	199.78
CH_4†	Transition zone	0.07	0.11*	0.03	0.02	< 0.01*	0.01	0.24
	Lacustrine zone	0.03	0.09	0.01	0.07	< 0.01	0.01	0.21
	Turbine	8.11	1.44	0.03	0.17	0.17	0.01	9.93
	Downstream	0.16	0.08	0.05	0.06	< 0.01	0.01	0.35
	Total	8.36	1.72	0.12	0.31	0.18	0.04	10.73
N_2O†	Transition zone	0.12	0.23*	0.31	0.19	< 0.01*	0.01	0.86
	Lacustrine zone	0.13	0.20	0.20	0.18	< 0.01	< 0.01	0.71
	Turbine	0.89	2.89	0.74	0.52	0.02	0.01	5.07
	Downstream	0.20	0.48	0.43	0.26	< 0.01	< 0.01	1.37
	Total	1.34	3.80	1.68	1.16	0.03	0.02	8.01

*Data were estimated assuming average GHG concentrations of the transition zone equal that of the lacustrine zone, as field samples were not always collected. The duration of each season/period in a year was 78 d for spring, 107 d for summer, 61 d for fall, 90 d for winter, 5 d for flood-rising period, and 24 d for flood-falling period.
†The emissions were converted to CO_2-equivalent (CO_2-eq). 1 g CH_4 = 27.0 g CO_2-eq, 1 g N_2O = 273.0 g CO_2-eq (IPCC 2021).

nitrogen inputs (Yan et al. 2023). Daily N_2O effluxes from the continuum during the spring flood-rising and flood-falling periods were 5.3 and 0.8 t CO_2-eq d^{-1}, respectively, much lower than for other periods (12.8–35.5 t CO_2-eq d^{-1}) (Supporting Information Table S2).

Discussion

Appreciable production of GHGs in the hypolimnion of SK reservoir occurred during the stratified (spring/summer, CO_2, CH_4, and N_2O) and mixed (autumn/winter, mainly as CO_2) periods (Figs. 2, 5), accompanied by consistent oxygen depletion (Fig. 1; Supporting Information Fig. S3). A similar deoxygenation-driven hypolimnetic mineralization is observed in many reservoirs and lakes (e.g., Kariba Reservoir, Lake Biwa) (Thottathil et al. 2013; Calamita et al. 2021). The $\Delta O_2/\Delta CO_2$ ratio is an indicator of the contribution of anaerobic processes, as anaerobic respiration produces relatively low ratios. Indeed, this indicator showed different ranges between the middle and bottom layers at S4 (Fig. 5). Aerobic-dominated aquatic ecosystems theoretically display a ΔO_2–ΔCO_2 relationship that falls roughly on a $1:-1$ line (Fig. 5d), which reflects the stoichiometry of glucose production and respiration (Vachon et al. 2020). Deviation from this theoretical metabolic $1:-1$ line is affected by combinations of biological, chemical, and physical processes. Our $\Delta O_2/\Delta CO_2$ ratios in the middle layer containing some oxygens were roughly around the $1:-1$ line, whereas ratios in the bottom layer, particularly in spring and late summer, showed a rightward shift relative to the $1:-1$ line (Fig. 5), indicating a microbially mediated anaerobic pathways producing CO_2 without concomitant consumption of O_2 (e.g., denitrification and acetoclastic methanogenesis) (Vachon et al. 2020).

Aerobic production of hypolimnetic CO_2: Temperature regulation

Oxygen in the hypolimnion of SK reservoir was not completely consumed from fall to early-stratified spring and during early-stratified summer after O_2 resupply by spring flooding (Fig. 1; Supporting Information Fig. S3). The middle layer of SK reservoir during late spring and late summer was in an aerobic state with some periods of hypoxia for near-bottom waters. Therefore, aerobic mineralization dominated hypolimnetic CO_2 production during these periods. In the aerobic spring period, the hypolimnetic in situ CO_2 production rate derived from oxygen utilization was 5.49 ± 1.83 μmol L^{-1} d^{-1} (Fig. 6), while the hypoxic water column CO_2 production rate based on laboratory incubation experiments was 4.58 ± 0.61 μmol L^{-1} d^{-1} (Fig. 3h). Hence, the sediment CO_2 production rate, estimated by difference, was 0.92 ± 1.28 μmol L^{-1} d^{-1}. This indicates that water column respiration was the major contributor to CO_2 production under aerobic conditions (Zhou et al. 2021*a*).

In situ CO_2 production rates during the warm summer were significantly higher than those during the other seasons (Fig. 6), suggesting a strong temperature regulation for (aerobic) CO_2 production in inland dark waters. A similar temperature regulation was observed for the humic-like fluorescent DOM ($FDOM_H$) component in SK reservoir, which is another product of deoxygenation-related microbial transformations (Qu et al. 2022). The higher

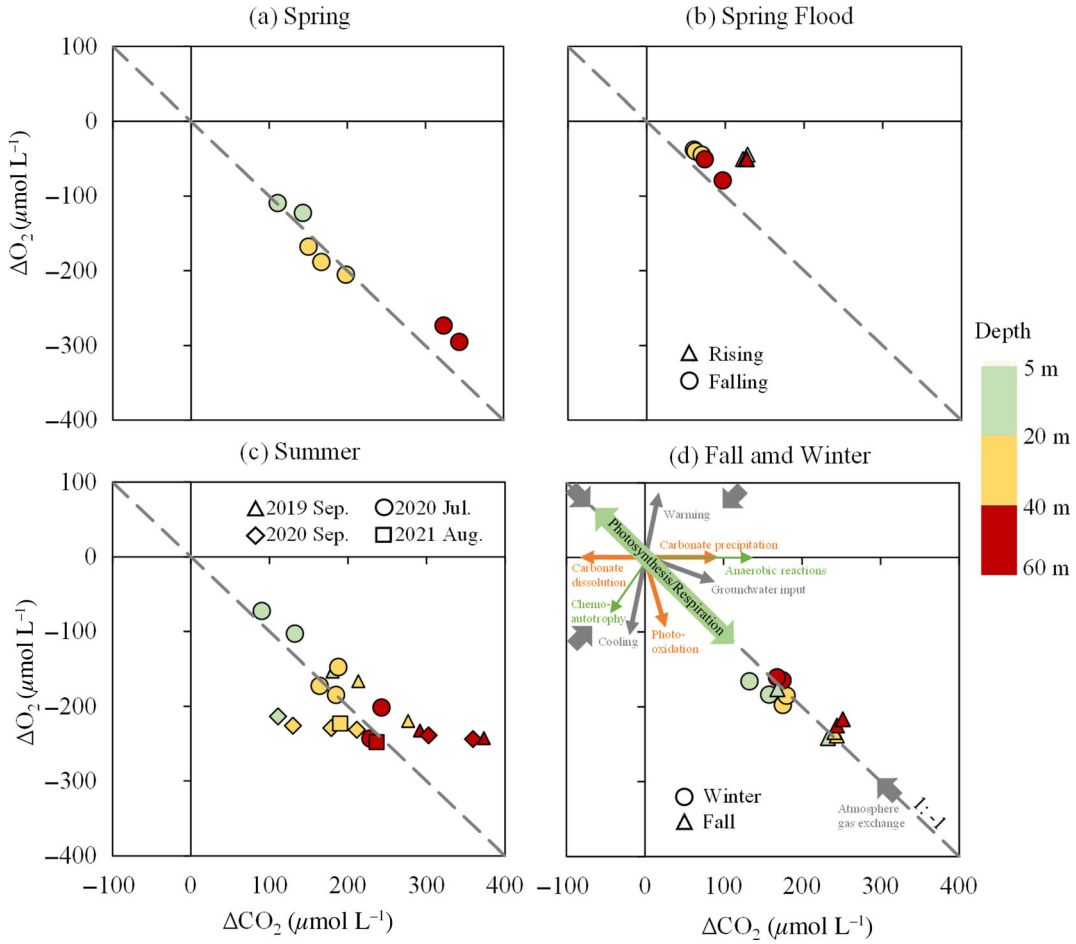

Fig. 5. O_2 departure from atmosphere equilibrium (ΔO_2) vs. excess CO_2 (ΔCO_2) in all periods (**a**: spring; **b**: spring flood; **c**: summer; **d**: fall and winter) below the euphotic zone at site S4 in SK reservoir. The arrows in (**d**) show the potential role of the different drivers (Vachon et al. 2020).

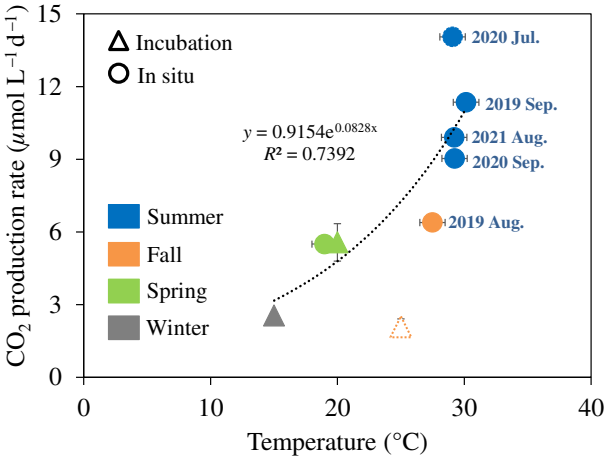

Fig. 6. Comparison of the relationship between CO_2 production rate based on incubations (triangles) and calculated from oxygen utilization (circles) and temperature in the hypolimnetic water column of SK reservoir. The fall incubation result (open triangle) was excluded from the regression analysis because a lack of organic substrate resupply might have limited respiration activity.

temperature facilitates a higher hypolimnetic OUR and, thus, the in situ CO_2 production rate in the warmer summer compared to the cooler spring (Fig. 6). This occurred despite the higher hypolimnetic oxygen consumption during the spring owing to a longer WRT. Therefore, variation in reservoir WRTs during periods of stratification may influence the production of CO_2 mainly through regulation of the hypolimnetic temperature.

To quantify the temperature sensitivity of CO_2 production, we estimated the Q_{10} value from 15°C to 30°C. The value of 2.3 obtained for aerobic CO_2 production in SK reservoir is at the center of Q_{10} values (0.1–4.0) reported for CO_2 production in streambed and lake sediments (Liikanen et al. 2002; Comer-Warner et al. 2018). Consequently, future warming would lead to higher CO_2 production in such reservoirs as more organic matter and oxygen will inevitably be consumed. Moreover, warming will likely enhance vertical stratification, thereby limiting oxygen availability and causing more severe hypoxia issues (Woolway et al. 2020), which would further enhance anaerobic CH_4 and N_2O production (discussed in the following section).

Late spring/summer stratification: Hypolimnetic anaerobic processes and GHG degassing

During late spring/summer stratification (Fig. 1b), the hypolimnion was anoxic (Fig. 1d). The rightward shift of $\Delta O_2/\Delta CO_2$ ratios in Fig. 5 indicates that there was anaerobic production of CO_2. Anaerobic decomposition of organic matter coupled with nitrate and sulfate reduction could raise ΔCO_2 (Salomão et al. 2008). The spring incubation experiment demonstrated that the bottom oxygen of SK reservoir could be quickly consumed (~ 5 d), creating an anaerobic environment with sustained CO_2 production (Fig. 3h). Notably, production of CH_4 and N_2O along with NO_3–N consumption was simultaneously observed (Fig. 2a,d; Supporting Information Fig. S7c), suggesting methanogenesis and denitrification in the bottom layer/sediments during late spring and summer. Anaerobic production of CH_4 in bottom waters during the spring was 0.19 μmol L^{-1} d^{-1} based on the incubation experiments (Fig. 3h). Thus, bottom-water (> 40 m) CH_4 production in SK reservoir during the spring was 94 mmol m^{-2}, much smaller than the CH_4 storage in the bottom layer (732 mmol m^{-2}) as estimated from the bottom-water CH_4 concentration increase (Fig. 2). This suggests that methanogenesis in sediments plays an important role in hypolimnetic CH_4 dynamics via sediment–water exchange.

During spring/summer stratification, methanogenesis could contribute 14.2–14.7% of the excess CO_2 produced in the bottom layer, and denitrification contributed 19.2–28.3% of excess CO_2 production, estimated by the theoretical stoichiometric ratios for methanogenesis ($\Delta CO_2/\Delta CH_4$: 1/1) and denitrification ($\Delta CO_2/\Delta NO_3^-$: 10/8) (Cai et al. 2003; Krumins et al. 2013). These estimates were determined from the differences between bottom and surface water concentrations of NO_3^- and CH_4. The $\Delta O_2/\Delta CO_2$ ratios after correction for methanogenesis and denitrification (late summer: −1.19; late spring: −1.23) were closer to the zero point and 1 : −1 line, further supporting the role of anaerobic processes in sustaining CO_2 production in the bottom-water layer during late spring/summer stratification. Notably, much longer hypolimnetic anaerobic conditions and stronger production of GHGs would occur if the thermal stratification was not broken by the large spring flood event.

CH_4 oxidation is a potentially important process in SK reservoir, as inferred from the sharp decline of CH_4 concentrations in the upper water column (Fig. 2a,d) (Soued and Prairie 2020). If all the methane produced diffused upward, most of it would be oxidized to carbon dioxide, which has a much lower GWP. However, turbine degassing provides an efficient pathway for CH_4 to bypass water column oxidation thus directly released to the atmosphere. In the SK reservoir, daily CH_4 effluxes due to turbine degassing varied from 0.4 to 104 t CO_2-eq d^{-1}, with a higher contribution to total CH_4 effluxes during stratified periods and the hypoxic spring (97%) and summer (84%) conditions than during mixed, oxic fall, and winter conditions (22–55%) (Table 1).

Priming effects enhance hypolimnion CO_2 production

The surface labile organic matter to the bottom layer for priming was possibly driven by hyperpycnal flow and/or overturning processes during mixed periods (Supporting Information Fig. S3b,c). The weak positive priming signals in fall and winter in the SK reservoir could be mainly due to little surface algal bloom events (Fig. 3). However, the obvious algal bloom events could support an active priming effect during stratified spring and possibly stratified summer. Algal bloom events produce large amounts of bio-labile organic materials (Qu et al. 2022), which may sink to the bottom layer and contribute to the formation of anaerobic conditions. Incubation experiments indicated that input of these fresh organic materials in spring could initiate a much stronger priming effect during anaerobic conditions than during mixed periods (Fig. 3), that is, stimulating the production of other GHG gases (CH_4 and N_2O) besides CO_2. The higher CO_2 production rate during early summer 2020 than other summer periods (Fig. 6) could be due to the hypolimnetic priming effect initiated by frequent algal blooms (Fig. 1f). Therefore, long-term in situ sensor monitoring of oxygen in the hypolimnion, especially the bottom layer, should be included in river observation system (RIOS) projects to better constrain the relationship of oxygen depletion with GHG production and emissions from reservoirs (Battin et al. 2023). Overall, this study highlights possible ways that priming might affect GHG emissions from reservoirs, but further observations and experiments are required to gain a more robust understanding.

Flooding events perturb GHG dynamics and longitudinal transport

There are regular late-spring flooding events in the Min River-SK reservoir system (Qu et al. 2022), which differentially alter the hypolimnetic GHG dynamics of the reservoir between its rising and falling periods. During the flood-rising period (18–22 May 2021), there was a rapid rise of DO accompanied by a 0.4 decrease in pH (from 6.8 to 6.4) (Supporting Information Fig. S8). Accordingly, the $\Delta O_2/\Delta CO_2$ was up above the 1 : −1 line (Fig. 6), largely due to a concurrent rapid increase in water temperature and catchment input of CO_2-rich water. The pH decrease might be due to the mixing of reservoir waters with lower-pH riverine waters during the storm runoff or chemical proton buffering effects as the replenishment of DO (8 mg L^{-1}) was faster than CO_2 degassing from the reservoir (Middelburg 2019). Higher temperatures result in lower CO_2 solubility, and a lower pH creates more CO_2 (from HCO_3), possibly contributing to more degassing (Carrillo et al. 2004). This mechanism is supported by the higher ΔCO_2 concentration during the rising period (130–137 μmol L^{-1}) than that during the falling period (66–106 μmol L^{-1}) when dilution dominated dissolved CO_2 dynamics due to strong flushing. Together with the sudden increase of fluvial runoff during the rising period, the daily CO_2 efflux from the SK reservoir was 3668 t CO_2-eq d^{-1}, which was 9–12 times greater

than that in fall and winter (Supporting Information Table S2). In addition, 36.7 t CO_2-eq d^{-1} of CH_4 and 5.3 t CO_2-eq d^{-1} of N_2O were released during the rising flood period. Large amounts of GHGs were flushed from the reservoir and contributed to a significant GHG efflux from turbine degassing and downstream river emissions.

During the flood-falling period (23 May–11 June 2021), $\Delta O_2/\Delta CO_2$ ratios in the hypolimnion shifted to the left and were closer to the 1 : −1 line (Fig. 5b). This could be due to the enhancement of aerobic respiration as average oxygen consumption rate was as high as 0.27 mg O_2 L^{-1} d^{-1} in the bottom layer (Supporting Information Fig. S8). The lowest hypolimnetic ΔCO_2 values (80.5 ± 13.9 μmol L^{-1}) within the annual timescale occurred during the falling period. This indicates a flushing-dilution mechanism controlling reservoir CO_2 dynamics over the course of the flood event. Dilution decreased CO_2 after the initial flushing of the reservoir CO_2 pool and slowed the oxygen consumption rate. Such a supply-limited phenomenon has been observed during El Nino-driven extreme flooding events (Qu et al. 2022) and could be a general pattern for strong flooding events (Gao et al. 2018). Nonetheless, the daily CO_2 efflux from the SK reservoir was 529 t CO_2-eq d^{-1} during the falling period, which was much less than the flood-rising period, but still higher than fall/winter efflux values (Supporting Information Table S1). In contrast, daily CH_4 and N_2O effluxes from the continuum during the falling period were only 4% and 14% of the CH_4 and N_2O efflux during the flood-rising period. Reoxygenation might depress their anaerobic production, leading to the low CH_4 and N_2O effluxes during the flood-falling period.

In total, the spring flood event contributed 28.7 Gg CO_2-eq. (28.5 Gg by CO_2), accounting for 13% of the annual GHG efflux (218.5 Gg CO_2-eq yr^{-1}) (Table 1). This indicates that spring floods provide a disproportionately large CO_2 efflux from subtropical reservoirs. In the future, more intense precipitation events associated with climate change could lead to more GHG emissions from riverine reservoir systems during flooding periods (Rozemeijer et al. 2021). This highlights the necessity of considering extreme weather events in global-scale assessments of GHG emissions (Battin et al. 2023).

Diurnal considerations for reservoir GHG budgets during algal bloom periods

Diurnal variations of in situ pCO_2 and CO_2 fluxes displayed distinct differences between seasons (Fig. 4; Supporting Information Fig. S5b). In contrast to the small fall and winter diurnal variations, relatively large diurnal pCO_2 variation was observed during algal bloom periods (spring: 83–3897 μatm; summer: 404–4210 μatm; flood falling: 55–2501 μatm) (Supporting Information Fig. S5b). The significant negative relationship between temperature-normalized pCO_2 and DO in surface water (Supporting Information Fig. S9) indicates that the photosynthesis–respiration balance rather than temperature had the strongest effect on diurnal variations (Macklin et al. 2018; Pu et al. 2020). As such, the reservoir served as a temporary sink for atmospheric CO_2 during certain daytime periods with high algal production. However, integrated over a 24-h period, it was a net CO_2 source even if there were frequent algal blooms (Supporting Information Fig. S10). This indicates that the SK reservoir during the algal bloom periods is a net heterotrophic system dominated by microbial respiration of allochthonous organic matter. Thus, given the considerable diurnal CO_2 variability, routine daytime surveys of pCO_2 could lead to a significant underestimate of water–air CO_2 fluxes from reservoirs (Calamita et al. 2021). The appreciable spatial variation of pCO_2 across the reservoir system during longitudinal boat underway measurements was largely due to variations in monitoring time (morning vs. evening). Therefore, the direct spatial comparison of pCO_2 patterns without suitable correction for diurnal CO_2 dynamics will induce considerable uncertainty.

Given these concerns, the in situ pCO_2 at each time point for a certain location was corrected for diurnal variability by assuming that the magnitude of the diurnal pCO_2 variation across the reservoir-downstream river continuum was similar to that at monitoring station S4 (Supporting Information Text S9). Correspondingly, the 24-h-averaged water–air CO_2 flux at each location (at 0.1 m intervals) was estimated. This correction indicated that the water–air CO_2 flux in 65.6%, 99.4%, and 89.7% of the reservoir area in spring, summer, and flood-falling periods were underestimated (Supporting Information Fig. S10a,d,e) with maximum daily pCO_2 differences of 54, 39, and 26 μatm, respectively (Supporting Information Fig. S5b). In contrast, corrected water–air CO_2 fluxes were similar to the in situ values during fall and winter (Supporting Information Fig. S10b,c), but experienced relatively high values due to overturn transport of hypolimnetic CO_2-rich water to the surface (Fig. 1) (Pu et al. 2020). Thus, in situ, high-frequency monitoring and correction for diurnal variation of GHG concentrations during algal bloom periods are crucial for better constraining global estimates of GHG emissions from hydroelectric reservoirs and other biologically active aquatic ecosystems.

Carbon neutrality of reservoirs: Relative importance of GHG emissions vs. RDOC storage

Previous studies found that hypolimnetic microbial oxygen depletion in reservoirs and lakes enhances the production and storage of RDOC in inland waters, thereby serving as an important carbon sink (Thottathil et al. 2013; Qu et al. 2022). Observations from the subtropical SK reservoir and other reservoirs/lakes (e.g., tropical Kariba Reservoir [Zambia/Zimbabwe], temperate Lake Biwa [Japan]) indicate that this process also intensifies the production and outgassing of GHGs, thus serving as a carbon source to the atmosphere (Thottathil et al. 2013; Calamita et al. 2021; Ran et al. 2022). The alleviation of seasonal hypolimnetic hypoxia by engineering measures could appreciably reduce GHG emissions in such reservoirs.

Therefore, carbon neutrality related to reservoir hypoxia depends on the relative importance of its source vs. sink processes (Chen et al. 2022). The water–air GHG fluxes for the SK reservoir-downstream river continuum indicate that it was a year-round source of GHGs (i.e., sources > sinks) (Table 1). Thus, organic matter transformations by reservoir oxygen consumption were not a net carbon sink process.

RDOC is a by-product of microbial respiration associated with oxygen consumption (Hayase et al. 1988). If the substrate of respiration were only from in situ primary production within the reservoir, there could be some storage of RDOC components, making oxygen depletion a net carbon sink process. However, overall SK reservoir is a substantial source of CO_2 because of the respiration of degradable allochthonous organic matter, in particular, during flood events. Moreover, the priming effect from relatively labile organic matter, both external and locally produced, enhanced CO_2 production through extra consumption of recalcitrant organic matter (Fig. 3). The formation of anaerobic conditions under thermal stratification further promotes production and outgassing (through turbine and downstream river emissions) of CH_4 and N_2O, which have a much stronger GWP than CO_2 (Hayase et al. 1988; He et al. 2021; Shenoy et al. 2021). Although the storage of RDOC originating from local production is a sink of carbon, it is clear that it does not offset the emissions of GHGs.

Projected future temperature increases could prolong stratified periods and strengthen the thermal stratification of reservoirs (Zhang et al. 2014), thereby enhancing GHG production in the hypolimnion of inland waters (Fig. 6). The intensification of thermal stratification and oxygen consumption could further increase the occurrence and volume of hypolimnetic anaerobic waters resulting in enhanced production of CH_4 and N_2O. Outgassing of these GHGs by reservoir outflows under shorter WRTs (i.e., flood events) could, therefore, enhance the GHG source intensity of the reservoir-river continuum. With ongoing dam construction for hydroelectric reservoirs, progressively more fluvial organic matter could be degraded in reservoirs instead of in estuaries (Maher and Eyre 2012), thus changing the carbon balance across land–air–ocean interfaces.

Data availability statement

The data that supports the findings of this study are available in the Supporting Information Material of this article.

References

Abril, G., and others. 2005. Carbon dioxide and methane emissions and the carbon budget of a 10-year old tropical reservoir (Petit Saut, French Guiana). Global Biogeochem. Cycles **19**: GB4007. doi:10.1029/2005GB002457

Atkins, M. L., I. R. Santos, S. Ruiz-Halpern, and D. T. Maher. 2013. Carbon dioxide dynamics driven by groundwater discharge in a coastal floodplain creek. J. Hydrol. **493**: 30–42. doi:10.1016/j.jhydrol.2013.04.008

Barros, N., J. J. Cole, L. J. Tranvik, Y. T. Prairie, D. Bastviken, V. L. M. Huszar, P. del Giorgio, and F. Roland. 2011. Carbon emission from hydroelectric reservoirs linked to reservoir age and latitude. Nat. Geosci. **4**: 593–596. doi:10.1038/ngeo1211

Battin, T. J., and others. 2023. River ecosystem metabolism and carbon biogeochemistry in a changing world. Nature **613**: 449–459. doi:10.1038/s41586-022-05500-8

Bianchi, T. S. 2011. The role of terrestrially derived organic carbon in the coastal ocean: A changing paradigm and the priming effect. Proc. Natl. Acad. Sci. USA **108**: 19473–19481. doi:10.1073/pnas.1017982108

Cai, W. J., Y. Wang, J. Krest, and W. Moore. 2003. The geochemistry of dissolved inorganic carbon in a surficial groundwater aquifer in North Inlet, South Carolina, and the carbon fluxes to the coastal ocean. Geochim. Cosmochim. Acta **67**: 631–639. doi:10.1016/S0016-7037(02)01167-5

Calamita, E., A. Siviglia, G. M. Gettel, M. J. Franca, R. S. Winton, C. R. Teodoru, M. Schmid, and B. Wehrli. 2021. Unaccounted CO_2 leaks downstream of a large tropical hydroelectric reservoir. Proc. Natl. Acad. Sci. USA **118**: e2026004118. doi:10.1073/pnas.2026004118

Carey, C. C., J. P. Doubek, R. P. McClure, and P. C. Hanson. 2018. Oxygen dynamics control the burial of organic carbon in a eutrophic reservoir. Limnol. Oceanogr.: Lett. **3**: 293–301. doi:10.1002/lol2.10057

Carey, C. C., and others. 2022. Anoxia decreases the magnitude of the carbon, nitrogen, and phosphorus sink in freshwaters. Glob. Change Biol. **28**: 4861–4881. doi:10.1111/gcb.16228

Carrillo, C. J., R. C. Smith, and D. M. Karl. 2004. Processes regulating oxygen and carbon dioxide in surface waters west of the Antarctic Peninsula. Mar. Chem. **84**: 161–179. doi:10.1016/j.marchem.2003.07.004

Chen, H., and others. 2022. Carbon and nitrogen cycling on the Qinghai-Tibetan Plateau. Nat. Rev. Earth Environ. **3**: 701–716. doi:10.1038/s43017-022-00344-2

Comer-Warner, S. A., P. Romeijn, D. C. Gooddy, S. Ullah, N. Kettridge, B. Marchant, D. M. Hannah, and S. Krause. 2018. Thermal sensitivity of CO_2 and CH_4 emissions varies with streambed sediment properties. Nat. Commun. **9**: 2803. doi:10.1038/s41467-018-04756-x

Deemer, B. R., and others. 2016. Greenhouse gas emissions from reservoir water surfaces: A new global synthesis. BioScience **66**: 949–964. doi:10.1093/biosci/biw117

Fearnside, P. M. 2002. Greenhouse gas emissions from a hydroelectric reservoir (Brazil's Tucuruí Dam) and the energy policy implications. Water Air Soil Pollut. **133**: 69–96. doi:10.1023/A:1012971715668

Gao, X. J., N. W. Chen, D. Yu, Y. Q. Wu, and B. Q. Huang. 2018. Hydrological controls on nitrogen (ammonium

versus nitrate) fluxes from river to coast in a subtropical region: Observation and modeling. J. Environ. Manag. **213**: 382–391. doi:10.1016/j.jenvman.2018.02.051

Guenet, B., M. Danger, L. Abbadie, and G. Lacroix. 2010. Priming effect: Bridging the gap between terrestrial and aquatic ecology. Ecology **91**: 2850–2861. doi:10.1890/09-1968.1

Guérin, F., G. Abril, D. Serça, C. Delon, S. Richard, R. Delmas, A. Tremblay, and L. Varfalvy. 2007. Gas transfer velocities of CO_2 and CH_4 in a tropical reservoir and its river downstream. J. Mar. Syst. **66**: 161–172. doi:10.1016/j.jmarsys.2006.03.019

Han, Q., B. Wang, C. Q. Liu, F. Wang, X. Peng, and X. L. Liu. 2018. Carbon biogeochemical cycle is enhanced by damming in a karst river. Sci. Total Environ. **616–617**: 1181–1189. doi:10.1016/j.scitotenv.2017.10.202

Hayase, K., H. Tsubota, I. Sunada, S. Goda, and H. Yamazaki. 1988. Vertical-distribution of fluorescent organic-matter in the North Pacific. Mar. Chem. **25**: 373–381. doi:10.1016/0304-4203(88)90117-X

He, C., and others. 2021. Mechanism of nitrous oxide (N_2O) production during thermal stratification of a karst, deep-water reservoir in southwestern China. J. Clean. Prod. **303**: 127076. doi:10.1016/j.jclepro.2021.127076

IPCC. 2021. Climate change 2021: The physical science basis. Contribution of working group I to the sixth assessment report of the Intergovernmental Panel on Climate Change.

Krumins, V., M. Gehlen, S. Arndt, P. van Cappellen, and P. Regnier. 2013. Dissolved inorganic carbon and alkalinity fluxes from coastal marine sediments: Model estimates for different shelf environments and sensitivity to global change. Biogeosciences **10**: 371–398. doi:10.5194/bg-10-371-2013

Kumar, A., T. Yang, and M. P. Sharma. 2019. Greenhouse gas measurement from Chinese freshwater bodies: A review. J. Clean. Prod. **233**: 368–378. doi:10.1016/j.jclepro.2019.06.052

Li, Y., and others. 2022. Changes in water chemistry associated with rainstorm events increase carbon emissions from the inflowing river mouth of a major drinking water reservoir. Environ. Sci. Technol. **56**: 16494–16505. doi:10.1021/acs.est.2c06405

Liikanen, A., T. Murtoniemi, H. Tanskanen, T. Väisänen, and P. J. Martikainen. 2002. Effects of temperature and oxygen availability on greenhouse gas and nutrient dynamics in sediment of a eutrophic mid-boreal lake. Biogeochemistry **59**: 269–286. doi:10.1023/A:1016015526712

Liu, H., Q. Zhang, G. G. Katul, J. J. Cole, F. S. Chapin, and S. MacIntyre. 2016. Large CO_2 effluxes at night and during synoptic weather events significantly contribute to CO_2 emissions from a reservoir. Environ. Res. Lett. **11**: 064001. doi:10.1088/1748-9326/11/6/064001

Lu, S., W. Dai, Y. Tang, and M. Guo. 2020. A review of the impact of hydropower reservoirs on global climate change. Sci. Total Environ. **711**: 134996. doi:10.1016/j.scitotenv.2019.134996

Maavara, T., R. Lauerwald, P. Regnier, and P. van Cappellen. 2017. Global perturbation of organic carbon cycling by river damming. Nat. Commun. **8**: 15347. doi:10.1038/ncomms15347

Macklin, P. A., I. Suryaputra, D. T. Maher, and I. R. Santos. 2018. Carbon dioxide dynamics in a lake and a reservoir on a tropical island (Bali, Indonesia). PloS One **13**: e0200948. doi:10.1371/journal.pone.0198678

Maher, D. T., and B. D. Eyre. 2012. Carbon budgets for three autotrophic Australian estuaries: Implications for global estimates of the coastal air-water CO_2 flux. Glob. Biogeochem. Cycles **26**: GB1032. doi:10.1029/2011GB004075

Middelburg, J. J. 2019. Marine carbon biogeochemistry: A primer for earth system scientists. Springer Cham. doi:10.1007/978-3-030-10822-9

Paranaíba, J. R., N. Barros, R. M. Almeida, A. Linkhorst, R. Mendonça, R. D. Vale, F. Roland, and S. Sobek. 2021. Hotspots of diffusive CO_2 and CH_4 emission from tropical reservoirs shift through time. J. Geophys. Res.: Biogeosci. **126**: e2020JG006014. doi:10.1029/2020JG006014

Pu, J., J. Li, T. Zhang, J. B. Martin, and D. Yuan. 2020. Varying thermal structure controls the dynamics of CO_2 emissions from a subtropical reservoir, south China. Water Res. **178**: 115831. doi:10.1016/j.watres.2020.115831

Qu, L., and others. 2022. Hypolimnetic deoxygenation enhanced production and export of recalcitrant dissolved organic matter in a large stratified reservoir. Water Res. **219**: 118537. doi:10.1016/j.watres.2022.118537

Ran, L., R. Yue, H. Shi, X. Meng, C. Ngai Chan, N. Fang, and Z. Shi. 2022. Seasonal and diel variability of CO_2 emissions from a semiarid hard-water reservoir. J. Hydrol. **608**: 127652. doi:10.1016/j.jhydrol.2022.127652

Richey, J. E., A. H. Devol, S. C. Wofsy, R. Victoria, and M. N. G. Riberio. 1988. Biogenic gases and the oxidation and reduction of carbon in Amazon River and floodplain waters. Limnol. Oceanogr. **33**: 551–561. doi:10.4319/lo.1988.33.4.0551

Rinta, P., D. Bastviken, M. van Hardenbroek, P. Kankaala, M. Leuenberger, J. Schilder, T. Stötter, and O. Heiri. 2015. An inter-regional assessment of concentrations and $\delta^{13}C$ values of methane and dissolved inorganic carbon in small European lakes. Aquat. Sci. **77**: 667–680. doi:10.1007/s00027-015-0410-y

Rozemeijer, J., R. Noordhuis, K. Ouwerkerk, M. D. Pires, A. Blauw, A. Hooijboer, and G. J. van Oldenborgh. 2021. Climate variability effects on eutrophication of groundwater, lakes, rivers, and coastal waters in the Netherlands. Sci. Total Environ. **771**: 145366. doi:10.1016/j.scitotenv.2021.145366

Salomão, M., J. Cole, C. Clemente, D. Silva, P. de Camargo, R. Victoria, and L. J. B. Martinelli. 2008. CO_2 and O_2

dynamics in human-impacted watersheds in the state of São Paulo, Brazil. Biogeochemistry **88**: 271–283. doi:10.1007/s10533-008-9210-y

Shenoy, D. M., S. Kurian, G. Shirodkar, H. Uskaikar, M. Gauns, and S. W. A. Naqvi. 2021. Impact of physical processes on oxygen loss and production of hydrogen sulphide and methane in a tropical freshwater reservoir. Environ. Sci. Pollut. Res. **28**: 39655–39667. doi:10.1007/s11356-021-13472-x

Soued, C., and Y. T. Prairie. 2020. The carbon footprint of a Malaysian tropical reservoir: Measured versus modelled estimates highlight the underestimated key role of downstream processes. Biogeosciences **17**: 515–527. doi:10.5194/bg-17-515-2020

Soued, C., J. A. Harrison, S. Mercier-Blais, and Y. T. Prairie. 2022. Reservoir CO_2 and CH_4 emissions and their climate impact over the period 1900–2060. Nat. Geosci. **15**: 700–705. doi:10.1038/s41561-022-01004-2

Tarroja, B., A. Aghakouchak, R. Sobhani, D. Feldman, S. Jiang, and S. Samuelsen. 2014. Evaluating options for balancing the water–electricity nexus in California: Part 2—Greenhouse gas and renewable energy utilization impacts. Sci. Total Environ. **497–498**: 711–724. doi:10.1016/j.scitotenv.2014.06.071

Thottathil, S. D., K. Hayakawa, Y. Hodoki, C. Yoshimizu, Y. Kobayashi, and S. Nakano. 2013. Biogeochemical control on fluorescent dissolved organic matter dynamics in a large freshwater lake (Lake Biwa, Japan). Limnol. Oceanogr. **58**: 2262–2278. doi:10.4319/lo.2013.58.6.2262

Vachon, D., and others. 2020. Paired O_2–CO_2 measurements provide emergent insights into aquatic ecosystem function. Limnol. Oceanogr.: Lett. **5**: 287–294. doi:10.1002/lol2.10135

Wang, J., and others. 2022. GeoDAR: Georeferenced global dams and reservoirs dataset for bridging attributes and geolocations. Earth Syst. Sci. Data **14**: 1869–1899. doi:10.5194/essd-14-1869-2022

Wang, S., K. M. Yeager, G. Wan, C. Q. Liu, F. Liu, and Y. Lü. 2014. Dynamics of CO_2 in a karst catchment in the southwestern plateau, China. Environ. Earth Sci. **73**: 2415–2427. doi:10.1007/s12665-014-3591-0

Wentzky, V. C., M. A. Frassl, K. Rinke, and B. Boehrer. 2019. Metalimnetic oxygen minimum and the presence of *Planktothrix rubescens* in a low-nutrient drinking water reservoir. Water Res. **148**: 208–218. doi:10.1016/j.watres.2018.10.047

Woolway, R. I., B. M. Kraemer, J. D. Lenters, C. J. Merchant, C. M. O'Reilly, and S. Sharma. 2020. Global lake responses to climate change. Nat. Rev. Earth Environ. **1**: 388–403. doi:10.1038/s43017-020-0067-5

Yan, J., and others. 2021. Interaction between oxygen consumption and carbon dioxide emission in a subtropical hypoxic reservoir, southeastern China. J. Geophys. Res.: Biogeosci. **126**: e2020JG006133. doi:10.1029/2020JG006133

Yan, R., F. Wang, Y. Wang, and N. Chen. 2023. Pollution abatement reducing the river N_2O emissions although it is partially offset by a warming climate: Insights from an urbanized watershed study. Water Res. **236**: 119934. doi:10.1016/j.watres.2023.119934

Yang, J., and others. 2023. Predominance of positive priming effects induced by algal and terrestrial organic matter input in saline lake sediments. Geochim. Cosmochim. Acta **349**: 126–134. doi:10.1016/j.gca.2023.04.005

Zagarese, H. E., and others. 2021. Patterns of CO_2 concentration and inorganic carbon limitation of phytoplankton biomass in agriculturally eutrophic lakes. Water Res. **190**: 116715. doi:10.1016/j.watres.2020.116715

Zhai, W., M. Dai, W. J. Cai, Y. Wang, and Z. Wang. 2005. High partial pressure of CO_2 and its maintaining mechanism in a subtropical estuary: The Pearl River estuary, China. Mar. Chem. **93**: 21–32. doi:10.1016/j.marchem.2004.07.003

Zhang, Y., Z. Wu, M. Liu, J. He, K. Shi, M. Wang, and Z. Yu. 2014. Thermal structure and response to long-term climatic changes in Lake Qiandaohu, a deep subtropical reservoir in China. Limnol. Oceanogr. **59**: 1193–1202. doi:10.4319/lo.2014.59.4.1193

Zhou, J., Z. Y. Zhu, H. T. Hu, G. L. Zhang, and Q. Q. Wang. 2021*a*. Clarifying water column respiration and sedimentary oxygen respiration under oxygen depletion off the Changjiang Estuary and adjacent East China Sea. Front. Mar. Sci. **7**: 623581. doi:10.3389/fmars.2020.623581

Zhou, Y., and others. 2021*b*. How hydrology and anthropogenic activity influence the molecular composition and export of dissolved organic matter: Observations along a large river continuum. Limnol. Oceanogr. **66**: 1730–1742. doi:10.1002/lno.11716

Acknowledgments

This research was supported by the National Natural Science Foundation of China (Grant Nos. 42276041, 41376082, and 42276040) and the Netherlands Earth System Science Center. Special thanks are given to Shuikou Hydropower Station for providing the cruise vessel and Zeyang Lu, Fenfang Wang, Yao Wang, Minxiang Zhu, Ruifeng Yan, and Yiqi Yu for their great assistance with sampling. The authors thank Mr. D.P. Huang and the crew for their assistance in YSI deployment/maintenance. We gratefully acknowledge Junou Du, Liguo Guo, Yan Li, Kunshan Jiang, and Pengjing He for their efforts in analytical analysis. We thank the anonymous reviewers for their valuable comments and suggestions.

Conflict of Interest

The authors declare no conflicts of interest.

Submitted 01 June 2023
Revised 29 December 2023
Accepted 22 February 2024

Associate editor: Yong Liu